Physics-Informed Acoustic Liner Optimization: Balancing Drag and Noise

Shahzad, H.; Hickel, S.; Modesti, D.

DOI
10.2514/1.J063677

Publication date
2024

Document Version
Final published version

Published in
AIAA Journal: devoted to aerospace research and development

AIAA JOURNAL
Vol. 62, No. 8, August 2024

Physics-Informed Acoustic Liner Optimization: Balancing Drag and Noise

Haris Shahzad,* Stefan Hickel,* and Davide Modesti*
Delft University of Technology, 2629 HS Delft, The Netherlands

https://doi.org/10.2514/1.J063677

Pore-resolved direct numerical simulations (DNS) of turbulent flows grazing over acoustic liners with aerodynamically and/or acoustically optimized orifice configurations are presented. The DNS explore a large parameter space, studying various families of orifice geometries, including the influence of orifice shape, orientation, and the number of orifices. All flow cases show an increase in drag compared to the smooth wall. However, the added drag can be reduced by as much as approximately 55% as compared to conventional acoustic liners by simply altering the shape of the orifice or its orientation, in the case of a noncircular orifice. Complementary acoustic simulations demonstrate that this reduced drag may be achieved while maintaining the same noise reduction properties over a wide range of frequencies.

Nomenclature

A	=	cross-sectional orifice area
a	=	major axis of ellipse
b	=	minor axis of ellipse
C_f	=	friction coefficient
c	=	speed of sound
d	=	orifice diameter
f	=	frequency of sound wave
f_r	=	liner resonance frequency
h	=	cavity depth
K	=	Darcy permeability
L_χ	=	domain size in χ direction
ℓ_T	=	virtual origin
M_b	=	bulk Mach number
M_∞	=	freestream Mach number
N_χ	=	grid points in χ direction
Re	=	Reynolds number
t	=	orifice thickness
u_b	=	bulk velocity
u_{cl}	=	centerline velocity
u_τ	=	friction velocity
V_c	=	cavity volume
V_o	=	orifices' volume
α	=	Forchheimer permeability
ΔU^+	=	Hama roughness function
δ	=	channel half-width
δ_v	=	viscous length scale
λ_c	=	cavity cross-section length/width
ν	=	kinematic viscosity
ρ	=	density
σ	=	facesheet porosity
τ_{ij}	=	Reynolds stresses
τ_w	=	wall shear stress
ω	=	angular frequency

I. Introduction

AIRCRAFT engines are the primary source of noise during takeoff and landing. To reduce noise, engine nacelles are equipped with noise control devices called acoustic liners. Acoustic liners are essentially an array of Helmholtz resonators, which consist of a large cavity with a small opening in the top plate. Acoustic liners are simple devices, and their working mechanism is based on the idea of dissipating noise by tuning their resonance frequency with the dominant frequency of the engine fan. They have the potential to attenuate noise by as much as 8–10 dB and are thus required on all aircraft jet engines.

Acoustic liners have been optimized primarily from an acoustic perspective [1–3]. From an aerodynamic perspective, however, they behave like surface roughness and contribute to an increase in aerodynamic drag. Our recent study [4] showed that acoustic liners are responsible for about a 70% drag increase per plane area compared to a hydraulically smooth wall at typical operating conditions. This aerodynamic penalty has been accepted as a necessary compromise.

The effect of acoustic liners on the background turbulent flow has only been studied recently, using both experiments [5–7] and numerical simulations [8,9]. Experimental studies are often characterized by large uncertainties in drag measurements, and numerical simulations of such surfaces are computationally expensive. Therefore, most studies have used simplifying assumptions to make the problem more approachable with numerical simulations. Several authors simulated the flow over a single acoustic liner cavity [9–11] or replaced the acoustic liner with an equivalent boundary condition [12–14]. As a result, estimates of the added drag reported in the literature have a massive spread, ranging from 3% up to 500%, depending on the numerical or experimental technique that was used [4].

Our group recently performed the first direct numerical simulations (DNSs) of fully resolved acoustic liner geometries [4], and we related the added drag to the wall-normal velocity fluctuations and the wall-normal Forchheimer permeability of the plate. Building on these findings, we showed that it is possible to predict the added drag of acoustic liners in operating conditions [4,15]. Hence, we are confident that better aerodynamic performance can be achieved by finding plate geometries that reduce the wall-normal velocity fluctuations induced by the orifices.

Howerton and Jones [16] studied different orifice configurations, changing the orifice shape and orientation, including rectangular orifices either parallel or perpendicular to the flow, and found that the perpendicular slot orifice performed better compared to the baseline circular orifices. The parallel slot orifice, on the other hand, despite having the same dimensions as the perpendicular slot orifice, had the highest added drag (at a freestream Mach number $M_\infty = 0.3$). Furthermore, Howerton and Jones noted that, despite changes in the orifice shape, the acoustic performance was largely unchanged, meaning that there is potential for reducing the added drag, without hampering the acoustic attenuation properties.

To the best of our knowledge, acoustic liners with varying orifice configurations have been studied only experimentally [16,17], and the physical rationale behind their choice of orifice configuration was missing. The objective of the current study is to show that it is possible to reduce this aerodynamic penalty while maintaining or improving acoustic noise attenuation. In this work, we use our recent findings [4] on scaling laws for the added drag to devise optimized

Received 23 October 2023; revision received 12 March 2024; accepted for publication 15 March 2024; published online 11 May 2024.

*Aerodynamics Group, Faculty of Aerospace Engineering, Kluyverweg 2.

acoustic liner geometries that reduce the added drag while having the same acoustic performance as the baseline configuration.

II. Methodology

A. Test Setup

We solve the compressible Navier–Stokes equations for a calorically perfect gas using the solver STREAmS [18,19] in a plane channel flow configuration. The computational domain is a rectangular box of size $L_x \times L_y \times L_z = 3\delta \times 2(\delta + h) \times 1.5\delta$, where δ is the channel half-width; h is the cavity depth; and x, y, and z denote the streamwise, wall-normal, and spanwise directions, respectively. This domain size is chosen based on previous studies on wall roughness and acoustic liners [4,20–23]. We perform DNS that fully resolves all turbulent length and time scales using a sixth-order spatial discretization and a third-order, three-stage Runge–Kutta scheme for time marching [24]. We carry out all simulations at friction Reynolds numbers $Re_\tau = \delta/\delta_v \approx 500$, where δ_v is the viscous length scale. Liner flow cases are complemented by a smooth-wall simulation at approximately the same friction Reynolds number and the same domain size. The simulations are performed at bulk Mach number $M_b = u_b/c_w = 0.3$, where u_b is the bulk flow velocity and c_w is the speed of sound at the wall. A uniform body force Π is added in the streamwise direction which is adjusted each time step to maintain a constant mass flow rate in the channel core. Conservation of mean momentum implies that the body force is related to the total drag experienced by the solid wall as $\Pi = \tau_w/\delta$, where τ_w is the drag per plane area. The acoustic liner geometry is handled using a ghost-point forcing immersed boundary method [25]. The immersed boundary method has been previously verified and validated and has been used to study a wide range of geometries [4,26]. Both walls are covered by an array of 8×4 acoustic liner cavities, as illustrated in Fig. 1. Each cavity has a square cross section with a side length $\lambda_c = 0.335\delta$ and depth $h = 0.5\delta$. The cavity walls have a thickness of 0.02δ. We use uniform mesh spacing in the streamwise and spanwise directions. In the wall-normal direction, the mesh is clustered toward the wall and coarsened toward the backplate and the channel center. A minimum of 26 mesh points is used to resolve the orifice diameter (or minor axis in the case of an ellipse). This resolution is well within the viscous spacing typically accepted in DNS, and it has been previously validated [4].

We wish to study the influence of orifice geometry on the aerodynamic and acoustic performance of a liner and compare it to the baseline configuration with circular straight holes that are common in most applications. For the baseline reference case (see Fig. 2b), we consider the geometry studied by Shahzad et al. [4] with porosity $\sigma = 0.322$, viscous-scaled diameter $d^+ = d/\delta_v \approx 40$, and a thickness to diameter ratio $t/d = 1$, where the orifice diameter for the baseline case is $d = 0.08\delta$. We chose the baseline liner geometry to be representative of acoustic liners in operating conditions, while also keeping a reasonable computational cost to perform a parametric study using DNS. The orifice size and facesheet thickness are in the range found on engine-mounted acoustic liners when scaled with the local boundary-layer thickness in landing conditions, as discussed by Shahzad et al. [4]. The cavity depth we use is smaller than in real applications; however, previous studies have reported that its influence on the added drag is negligible [5]. The porosity is higher than typically found on modern aircraft engines. However, in our recent study [4], we demonstrate that the relevant nondimensional parameter for quantifying the added drag is the viscous-scaled Forchheimer permeability, which is thus a more relevant nondimensional quantity than the porosity.

To compare the result of liner simulations with the smooth-wall data, we take into account the effect of the virtual origin ℓ_T, namely, the distance below the plate at which the flow perceives the equivalent smooth wall. More details on how the virtual origin is estimated are provided in our previous work [4]. In the following, quantities that are nondimensionalized by δ_v and u_τ are denoted by the $+$ superscript. The overline symbol $\overline{f}$ is used to indicate Reynolds averages, whereas the tilde $\tilde{f} = \overline{\rho f}/\overline{\rho}$ indicates Favre averaging, and the double prime symbol indicates fluctuations thereof $f'' = f - \tilde{f}$, where ρ is the density. As an example, with this notation, the ensemble-averaged Reynolds stress tensor is $\tau_{ij} = \overline{\rho}\,\widetilde{u_i'' u_j''}$, where $u_i = \{u_1, u_2, u_3\} = \{u, v, w\}$ are the streamwise, wall-normal, and spanwise velocity, respectively. All simulations are advanced forward in time until they reach a statistically stationary state, after which statistics are collected for at least $T_{\text{av}} u_\tau/\delta \approx 16$, where T_{av} is the averaging interval.

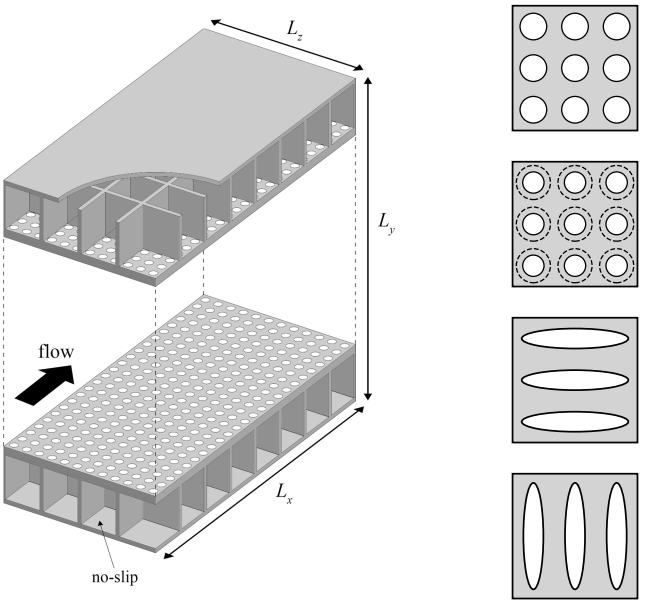

Fig. 1 Sketch of the computational domain.

B. Novel Configurations

The facesheet thickness and the cavity dimensions remain unchanged for all cases considered. The novel configurations proposed only differ in the orifice shape, size, and orientation. In an attempt to reduce the aerodynamic drag induced by acoustic liners, we pursue two ideas:

1) We aim at increasing the wall-normal Forchheimer permeability of the plate α_y. Although α_y has a complex dependency on the plate geometry, a first-order approximation is $\alpha_y \sim 1/(\sigma^2 t)$ [15], and therefore a reduction of the plate permeability will result in lower drag.

2) We take inspiration from riblets, namely, streamwise-aligned surface grooves that are able to reduce friction drag [27,28], and argue that the same surface anisotropy in the streamwise direction might be beneficial for acoustic liners.

Following these two hypotheses, we propose liner geometries that should be more efficient from an aerodynamic perspective and possibly retain the acoustic properties of the liner. Therefore, we change the orifice geometry while keeping constant the resonance frequency of the resonators $\omega_r = c_w\sqrt{A/tV_c}$, where A is the plane area of the orifice and V_c is the volume of the cavity. In this way, we aim to optimize the aerodynamic performance without compromising the acoustic properties.

Based on the first idea, we propose a *tapered-hole* configuration where the orifice has a smaller diameter at the top of the facesheet and a larger diameter at the bottom of the facesheet, such that the total volume of the orifice is constant and the resonance frequency of the liner, disregarding entry and exit effects, does not change. Entry and exit effects are included using empirical correction factors when determining the resonance frequency of the liner as they change the effective mass of air that oscillates in the orifice. For a canonical orifice shape, the correction is known and well documented [9,29–31]. Because entry/exit effects are accounted for by empirical corrections, our hypothesis can only be verified a posteriori through acoustic simulations at different frequencies. For the considered case

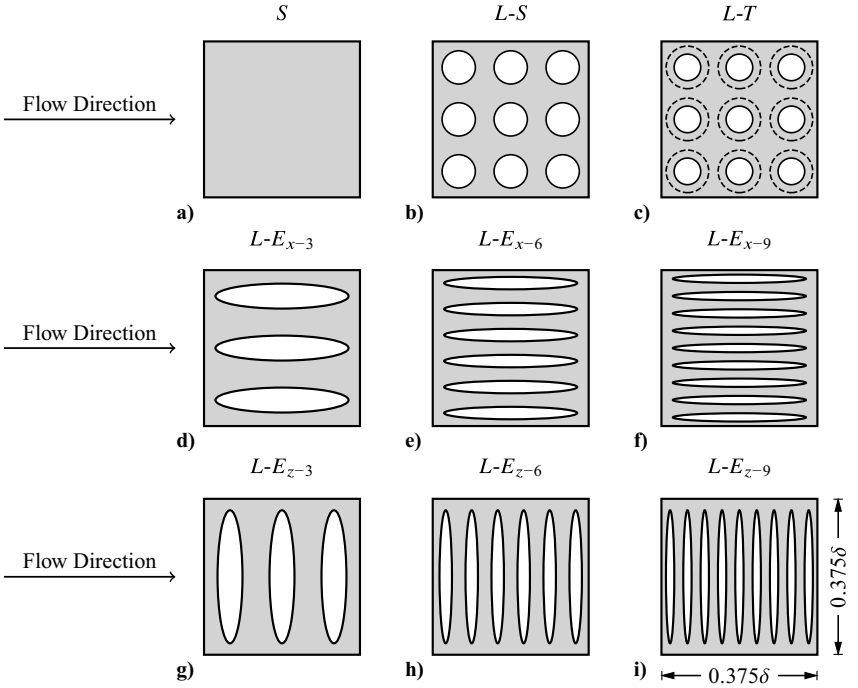

Fig. 2 Orifice configurations considered. All liner cases, except for case $L-T$, have a top surface open area ratio of $\sigma = 0.322$.

(The tapered hole case L-T), the orifice diameter increases continuously from $d = 0.064\delta$ at the top of the facesheet to $d = 0.1024\delta$ at the bottom of the facesheet.

Based on the second idea, we propose elliptical orifices that have the same porosity as the baseline liner, that is, $\sigma = 0.322$. The major axis of the ellipse is fixed at $a = 0.32\delta$, and the minor axis is calculated by assuming a constant porosity and depends on the number of orifices per cavity. For example, in the case of nine elliptical orifices per cavity (see Fig. 2f or Fig. 2i), the minor axis is $b = 0.02\delta$, and in the case of three elliptical orifices per cavity (see Fig. 2d or Fig. 2g), the minor is $b = 0.06\delta$, such that the porosity is always $\sigma = 0.322$.

In addition, the influence of the elliptical orifices' orientation is also studied. Although we expect that streamwise-aligned ellipses should minimize the added drag, previous experiments [16] have shown that rectangular slots perpendicular to the flow have lower drag compared to the canonical configuration. Therefore, we consider elliptical orifices with the major axis aligned with the streamwise or spanwise direction.

The geometries considered are shown in Fig. 2, and details of all flow cases are reported in Table 1. The naming of the flow cases is as follows: we use the letter S for the smooth-wall case and $L-C$ for the liner cases, where $C = \{S, T, E_{x-\chi}, E_{z-\chi}\}$ refers to the specific liner flow case. In particular, S, T, $E_{x-\chi}$, and $E_{z-\chi}$ are the baseline liner with straight orifice, tapered-orifice liner, streamwise-oriented ellipses, and spanwise-oriented ellipses, respectively, and χ is the number of ellipses per cavity.

III. Results

A. Aerodynamic Drag

Figure 3 shows the mean streamwise velocity profiles for all flow cases. We see that the mean velocity profile over acoustic liners is shifted downward as compared to the smooth wall. This downward shift is referred to as the ΔU^+, and it is directly related to the added drag through the exact relation [4]

$$\Delta D = 1 - \frac{C_f}{C_{f,s}} = 1 - \left(\frac{1}{1 - (\Delta U^+/\sqrt{2/C_{f,s}})}\right)^2 \tag{1}$$

where $C_f = 2\Pi\delta/(\rho U_c^2)$ is the friction coefficient, U_c is the mean streamwise velocity at the channel centerline, and the subscript s denotes smooth-wall values. The advantage of using ΔU^+, instead of the relative variation of the friction coefficient, is that ΔU^+ is independent from the Reynolds number; thus, it can be used as a drag measure in laboratory experiments or simulations which necessarily have a lower Reynolds number than acoustic liners in operating conditions. The effect of Reynolds number on ΔD is embedded in $C_{f,s}$, which can be easily estimated using smooth-wall formulas, allowing one to use low Reynolds number data to estimate the drag

Table 1 DNS dataset comprising smooth (S) and liner ($L-C$) cases

Flow case	Re_b	Re_τ	d_x^+	d_z^+	$K/t^2 \times 10^3$	$1/(\alpha t)$	Δx^+	$\Delta y^+_{\min}$	Δz^+	N_x	N_y	N_z	ΔU^+	$C_f \times 10^3$
S	18536	506.1	0	0	—	—	5.1	0.80	5.1	300	350	150	—	4.58
$L-S$	16528	505.3	40.4	40.4	6.33	0.127	1.5	0.80	1.5	1000	500	500	1.90	5.54
$L-T$	16984	515.8	33.0	33.0	17.0	0.156	1.3	0.81	1.3	1200	600	500	1.45	5.28
$L-E_{x-3}$	13124	492.8	29.6	157.7	7.32	0.0869	5.9	0.79	1.1	250	500	700	4.87	7.78
$L-E_{x-6}$	15602	501.5	15.0	160.5	2.23	0.0401	6.0	0.80	0.6	250	500	1300	2.33	5.80
$L-E_{x-9}$	17300	515.5	10.3	165.0	1.07	0.0217	6.2	0.82	0.4	250	500	2000	0.85	4.97
$L-E_{z-3}$	16104	510.0	163.2	30.6	7.32	0.0869	1.1	0.82	6.1	1400	500	125	2.17	5.70
$L-E_{z-6}$	16042	506.8	162.1	15.2	2.23	0.0401	0.6	0.81	6.1	2600	500	125	2.29	5.78
$L-E_{z-9}$	16670	515.6	165.0	10.3	1.07	0.0217	0.4	0.82	6.2	4000	500	125	1.90	5.54

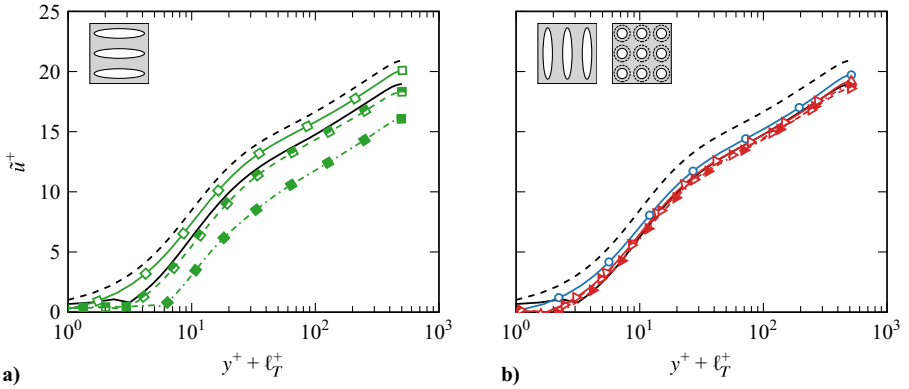

Fig. 3 Mean streamwise velocity for streamwise-oriented ellipses as a function of y^+. Novel geometries are compared to the smooth-wall flow case (dashed black line without symbols) and the baseline liner flow case (solid black line without symbols). The novel liner flow cases have the following line style: $L-T$ (circles), $L-E_{x-\chi}$ (squares), and $L-E_{z-\chi}$ (triangles). Different line types with symbols indicate the number of orifices per cavity: $\chi=3$ (dash-dotted line with filled symbols), $\chi=6$ (dashed line with half-filled symbols), and $\chi=9$ (solid line with empty symbols).

variation in operating conditions, as discussed by Shahzad et al. [4]. A positive ΔU^+ is correlated with a drag increase and represents a downward shift of the velocity profile with respect to the smooth wall. In Fig. 3, we note that all liner cases show a downward shift compared to the smooth wall ΔU^+, indicating that all cases increase drag. However, several liner geometries exhibit a lower ΔU^+ compared to the baseline case, demonstrating that modifying the orifice shape can result in a lower added drag. For convenience, the value of the Hama roughness function ΔU^+ and the friction coefficient are also reported in Table 1. Simulations are performed at bulk Reynolds number $Re_b = 2u_b\delta/\nu$. d_x and d_z are the lengths of the streamwise and spanwise axes of the orifices. Δx^+, $\Delta y^+_{\min}$, and Δz^+ are the viscous-scaled streamwise, minimum wall-normal, and spanwise mesh spacing.

Some elliptical orifice configurations show potential for decreasing the added drag. However, this depends both on the ellipse dimensions and orientation. For streamwise-oriented slots, the drag variation strongly depends on the spanwise size of the orifices. The narrow orifices of flow case $L-E_{x-9}$ lead to a substantially lower drag than the baseline case, whereas the wider slots of case $L-E_{x-3}$ result in a massive drag increase. It is interesting to note that the elliptical slots of $L-E_{x-9}$ have a spanwise width of size $d_z^+ \approx 10$, which is similar to the spacing of drag-reducing riblets [27]. For spanwise-oriented slots, ΔU^+ is less sensitive to the slots' size, and we find the same or a marginally lower drag than the baseline liner. These findings confirm the experiments of Howerton and Jones [16], who observed lower drag for spanwise-oriented rectangular slots. They found that streamwise-oriented rectangular slots increased drag compared to the baseline case; however, they did not investigate the effect of slot size, which might have been too large in viscous units to observe the *riblet-like* effect we report in this study. The tapered orifice also decreases drag compared to the baseline case. In this case, the improved performance can be traced back to the reduced superficial porosity experienced by the flow.

In a previous study, we related the added drag induced by acoustic liners to the wall-normal velocity fluctuations [4]; thus, we inspect instantaneous velocity realizations in wall-parallel planes at $y^+ + \ell_T^+ = 8$ in Figs. 4 and 5. For all liner cases, we note that near-wall streaks are disrupted and much shorter than on a smooth wall; see Fig. 4. The break-up of the near-wall streaks is particularly evident for case $L-E_{x-3}$ (Fig. 4g), where the near-wall flow deviates substantially from the typical organization found for the smooth wall (Fig. 4a).

For the baseline liner geometry, wall-normal velocity fluctuations are concentrated, primarily, around the orifice location, and the positions of the orifices are clearly visible in the contours of the wall-normal velocity; see Fig. 5b. This effect is more evident for cases $L-E_{x-3}$ and $L-E_{x-6}$, where the wall-normal velocity fluctuations in the near-wall region originate primarily from the orifices. The higher wall-normal velocity fluctuations for flow case $L-E_{x-3}$ are correlated with the significantly higher drag of this case.

Furthermore, we find that liner cases with lower drag present lower wall-normal velocity fluctuations and a more smooth-wall-like organization of the near-wall flow. These qualitative observations suggest that the correlation formulated by Shahzad et al. [4] that relates the added drag and the intensity of the wall-normal velocity fluctuations holds for all facesheet geometries under scrutiny.

For a more quantitative analysis, we further show the wall-normal Reynolds stress components $\tau_{22} = \overline{\rho}\,\widetilde{v''v''}$ in Figs. 6 and 7. It is clear that the wall-normal velocity fluctuations are not zero, irrespective of the case considered, above and below the facesheet. We find that flow cases that exhibit lower drag than the baseline liner show lower wall-normal velocity fluctuations in the near-wall region and below the facesheet (Fig. 6). The converse is true for cases that increase the added drag (Fig. 7).

B. Acoustic Attenuation

We have studied the aerodynamic drag of different orifice configurations and have identified several geometries that induce lower drag compared to the baseline liner with circular orifices. As acoustic liners are used to reduce engine noise, it is imperative to also test their acoustic performance. To do so, we study the noise attenuation properties of these novel configurations in the absence of grazing flow. A complete picture of the noise attenuation properties of aerodynamically optimized acoustic liner geometries would require including the influence of grazing flow. However, studies of acoustic liners without grazing flow have been extensively used to provide an initial estimation of their acoustic performance [32–34]. Simulations in the absence of grazing flow allow us to study the acoustic performance over a range of frequencies for all geometries considered at tractable computational cost.

Simulations are performed in a channel of size $L_x \times L_y \times L_z = 1250d \times (25d+h) \times 4.69d$, where d is the orifice diameter of the baseline liner and $h = 6.25d$ is the depth of the liner. The spanwise domain size corresponds to a single cavity, and periodic boundary conditions are applied in the spanwise direction. We apply no-slip isothermal boundary conditions on the top and bottom walls and place acoustic liners at the bottom wall of the channel. An array of 40×1 acoustic liner cavities is placed between $x_s = 500d$ and $x_e = 687.5d$. The geometries of the liners are the same as those considered when studying the aerodynamic performance. The resonance frequency of the system is expected to be approximately $f_r \approx 0.028c/d$. However, the correction due to the pressure field, particularly for the geometries considered in the paper, is difficult to estimate. We therefore test the performance of the novel geometries over a range of frequencies from $f/f_r = 0.5$ to $f/f_r = 1.5$ at a Reynolds number $Re_c = 800$ based on the orifice diameter and speed of sound. We verified that, although the absolute sound attenuation of these liners changes, the relative sound attenuation, compared to the baseline acoustic liner, does not depend on the Reynolds number.

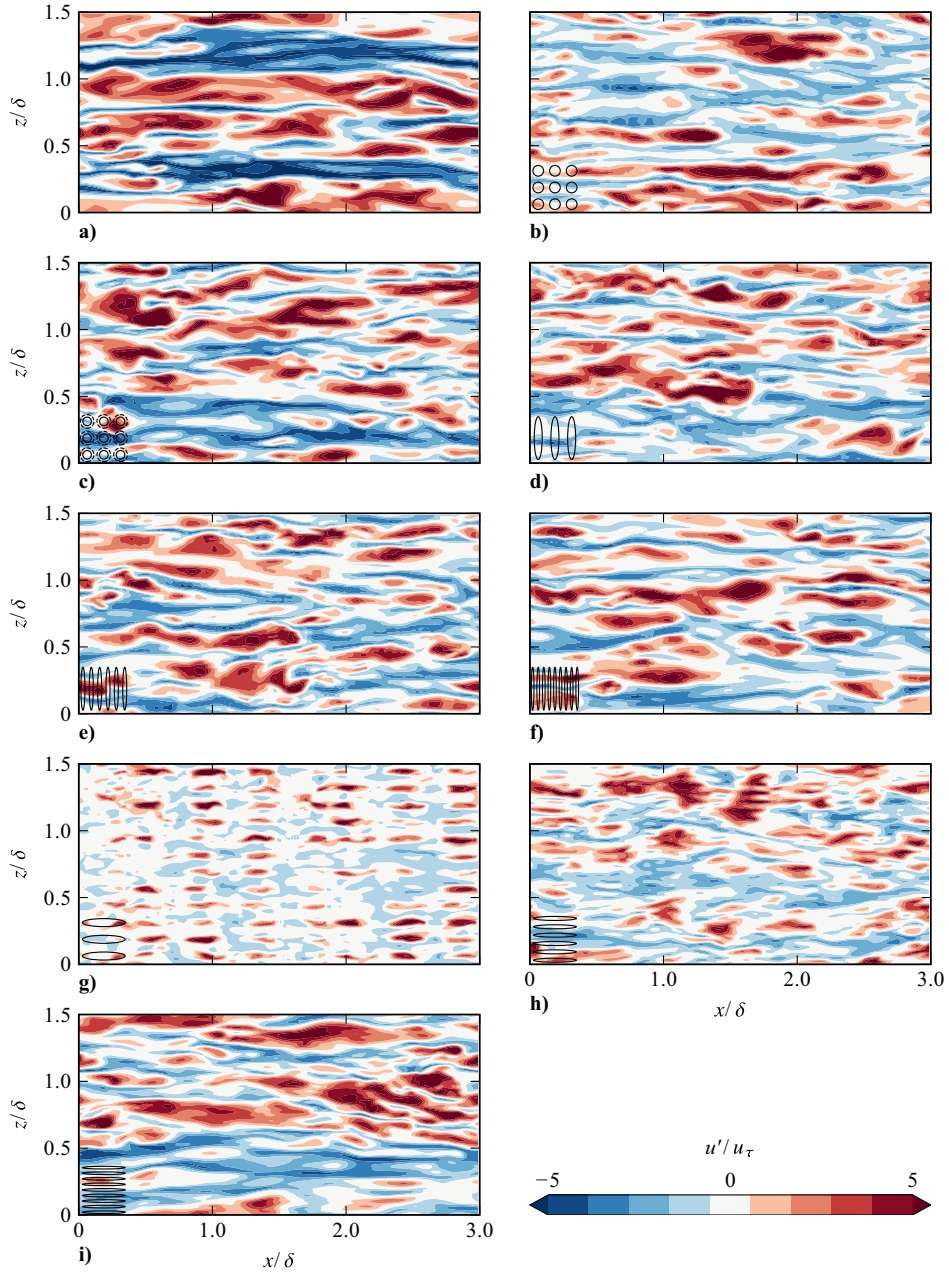

Fig. 4 Streamwise velocity fluctuations on a wall-parallel plane at $y^+ + \ell_T^+ = 8$ for cases a) S, b) $L - S$, c) $L - T$, d) $L - E_{z-3}$, e) $L - E_{z-6}$, f) $L - E_{z-9}$, g) $L - E_{x-3}$, h) $L - E_{x-6}$, and i) $L - E_{x-9}$.

Figure 8 shows an instantaneous snapshot of the pressure for the smooth-wall case and the baseline liner for the case with $f = f_r$. Figure 9 also shows how the instantaneous pressure field changes as the forcing frequency is changed. As the frequency of the acoustic wave is tuned to the resonant frequency of the liner, we see a significant attenuation of the acoustic wave over the liner. The amplitude of the pressure fluctuations toward the end of the acoustic liner is much lower than over the smooth wall, where the fluid viscosity is the only dissipative mechanism.

Figure 10 compares the sound pressure level (SPL) evolution of the acoustic wave for all the liner configurations and the smooth wall for the case with $f = f_r$. Although there is a clear SPL reduction for all configurations as compared to the smooth wall, some geometries perform better than others when evaluated against the baseline liner. This is true for the SPL loss over the entire frequency range considered; see Fig. 11. Cases $L - E_{x-3}$ and $L - E_{z-3}$ offer very similar acoustic noise attenuation over the entire frequency range; however, the narrow orifices of cases $L - E_{x-6}$, $L - E_{z-6}$, $L - E_{x-9}$, and $L - E_{z-9}$, which helped reduce drag, appear to inhibit acoustic noise attenuation. Cases $L - E_{x-6}$ and $L - E_{z-6}$ show similar noise attenuation properties at frequencies other than $f = 0.75 f_r$, whereas cases $L - E_{x-9}$ and $L - E_{z-9}$ show significantly lower attenuation throughout the frequency range. The tapered-hole configuration provides comparable acoustic noise attenuation as compared to the standard acoustic liner. Figure 11 also shows that the effective resonance frequency is about 25% lower than the nominal one, which we estimated disregarding entrance and exit effects. Notably, the resonant frequency appears to be about the same for all orifice shapes, suggesting that the required correction for entrance and exit effects is similar for all orifice shapes. The tapered holes therefore not only improve the aerodynamic performance of the liner but also perform well acoustically. The elliptical orifices, however, depending upon the width of the orifice, may or may not have a detrimental influence on acoustic noise attenuation.

IV. Conclusions

Several novel orifice geometries for acoustic liners, some of which reduce aerodynamic drag without compromising the acoustic

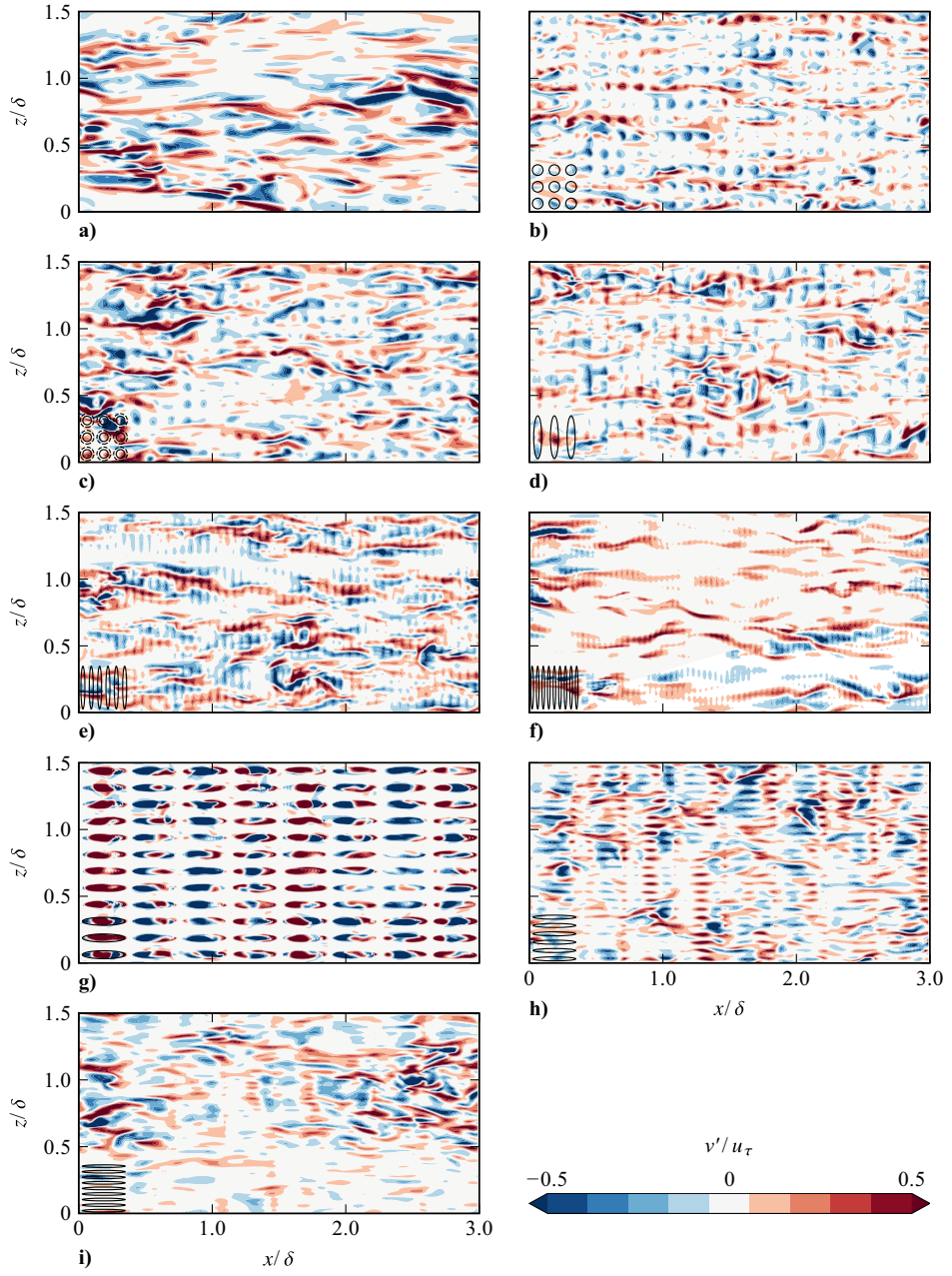

Fig. 5 Wall-normal velocity fluctuations on a wall-parallel plane at $y^+ + \ell_T^+ = 8$ for cases a) S, b) $L - S$, c) $L - T$, d) $L - E_{z-3}$, e) $L - E_{z-6}$, f) $L - E_{z-9}$, g) $L - E_{x-3}$, h) $L - E_{x-6}$, and i) $L - E_{x-9}$.

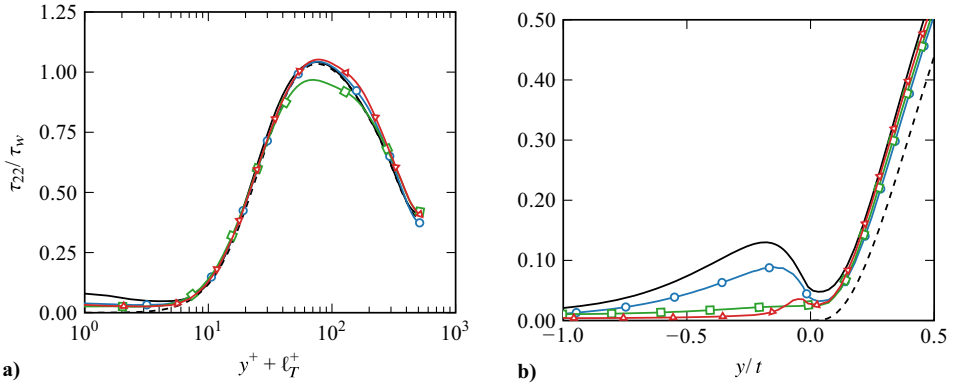

Fig. 6 Wall-normal Reynolds stress τ_{22} a) as a function of y^+ and b) as a function of y/t. Line types and symbols are as in Fig. 3.

performance, were proposed. The idea behind the aerodynamically optimized geometries is based on flow physics, which allows restriction of the vast parameter space that one could explore. The aerodynamic performance of the novel geometries is scrutinized based on direct numerical simulations of fully resolved acoustic liner arrays in a turbulent channel flow. It was found that tapered

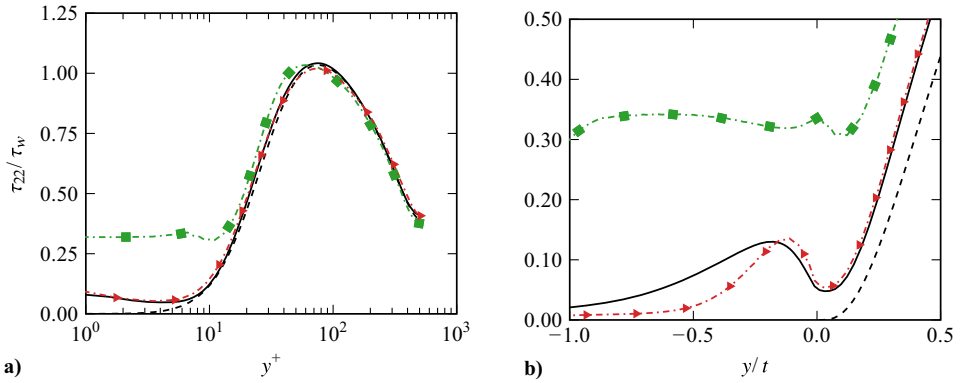

Fig. 7 Wall-normal Reynolds stress τ_{22} a) as a function of y^+ and b) as a function of y/t. Line types and symbols are as in Fig. 3.

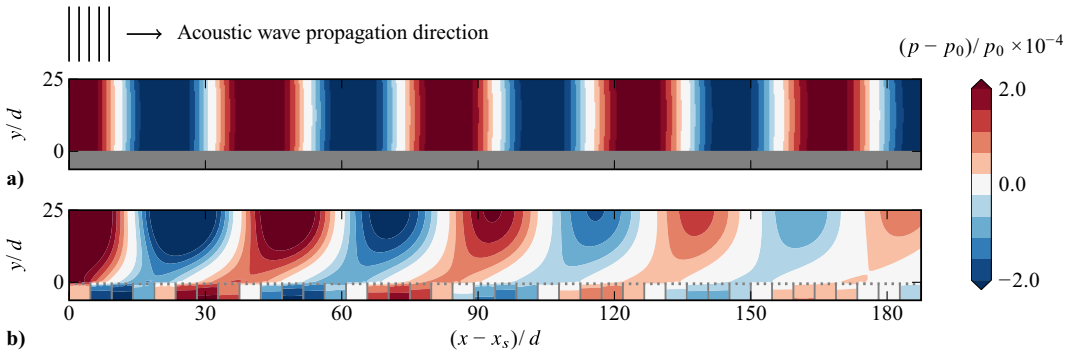

Fig. 8 Instantaneous pressure fluctuations over a) the smooth wall and b) the baseline liner; p_0 is the reference thermodynamic pressure, and x_s is the streamwise location where the liners start. The frequency of the sound waves is $f/f_r = 1$.

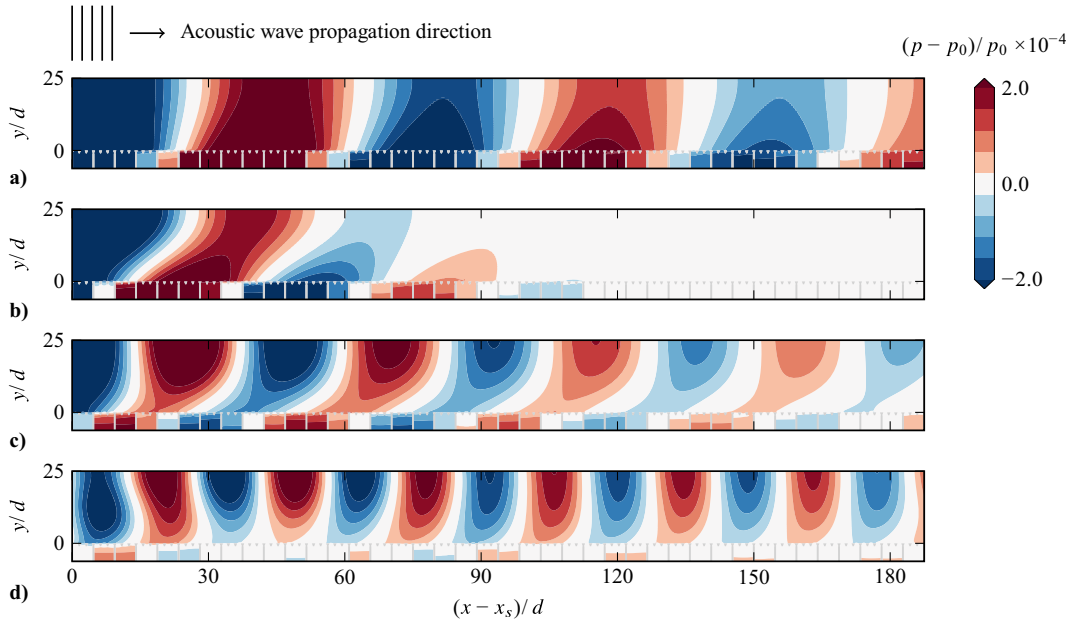

Fig. 9 Instantaneous pressure fluctuations for the tapered orifice configuration for various acoustic wave frequencies a) $f/f_r = 0.5$, b) 0.75, c) 1.0, and d) 1.5.

circular orifices minimize drag compared to a baseline acoustic liner by reducing the apparent porosity at the surface of the facesheet, whereas replacing the circular holes with elliptical slots can lead to a substantially lower drag if the minor axis of the ellipse is sufficiently thin in viscous units. It was found that, despite the very different configurations tested, all optimized geometries work by reducing the interaction of the flow above and below the surface of the facesheet, which is confirmed by the reduced wall-normal velocity fluctuations in the proximity of the facesheet.

The acoustic performance of the proposed liner configurations was also tested, and it was found that the thin elliptical slots have substantially reduced acoustic performance compared to a baseline liner; therefore, the improved aerodynamic benefit comes at the cost of lower noise reduction. The tapered-hole configuration has slightly

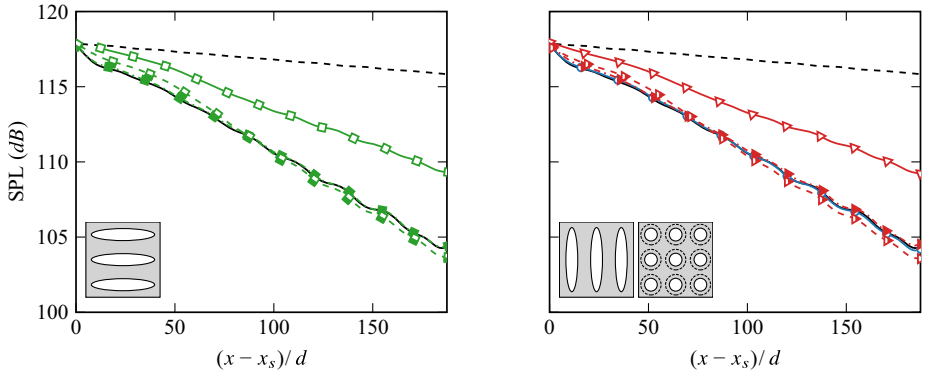

Fig. 10 Sound pressure level as a function of the streamwise distance from the start of the liners. Line types and symbols are as in Fig. 3.

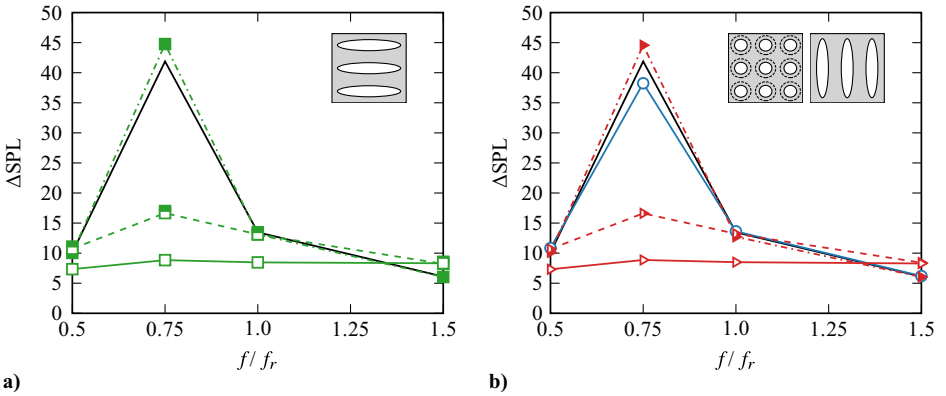

Fig. 11 Sound pressure level as a function of the forcing frequency. Line types and symbols are as in Fig. 3.

better noise attenuation properties than the baseline liner while offering substantially lower aerodynamic drag, and it is therefore superior from both an aerodynamic and an acoustic perspective. In addition, tapered holes are easy to manufacture and therefore represent a viable modification to be implemented in existing designs.

Acknowledgments

We acknowledge EuroHPC for awarding us access to Meluxina, at LuxProvide, Luxembourg. DNS data is available at https://doi.org/10.4121/1b59fc2b-d837-4479-836e-810aa5b0db3d.

References

[1] Sivian, L. J., "Acoustic Impedance of Small Orifices," *Journal of the Acoustical Society of America*, Vol. 7, No. 2, 1935, pp. 94–101. https://doi.org/10.1121/1.1915795

[2] Ingård, U., and Labate, S., "Acoustic Circulation Effects and the Nonlinear Impedance of Orifices," *Journal of the Acoustical Society of America*, Vol. 22, No. 2, 1950, pp. 211–218. https://doi.org/10.1121/1.1906591

[3] Mann, A., Perot, F., Kim, M.-S., and Casalino, D., "Characterization of Acoustic Liners Absorption Using a Lattice-Boltzmann Method," AIAA Paper 2013-2271, 2013. https://doi.org/10.2514/6.2013-2271

[4] Shahzad, H., Hickel, S., and Modesti, D., "Turbulence and Added Drag over Acoustic Liners," *Journal of Fluid Mechanics*, Vol. 965, June 2023, Paper A10. https://doi.org/10.1017/jfm.2023.397

[5] Howerton, B. M., and Jones, M. G., "Acoustic Liner Drag: A Parametric Study of Conventional Configurations," AIAA Paper 2015-2230, 2015. https://doi.org/10.2514/6.2015-2230

[6] Howerton, B. M., and Jones, M. G., "A Conventional Liner Acoustic/Drag Interaction Benchmark Database," AIAA Paper 2017-4190, 2017. https://doi.org/10.2514/6.2017-4190

[7] Gustavsson, J., Zhang, Y., Cattafesta, L. N., and Kreitzman, J. R., "Acoustic Liner Drag Measurements," AIAA Paper 2019-2683, 2019. https://doi.org/10.2514/6.2019-2683.c1

[8] Scalo, C., Bodart, J., and Lele, S. K., "Compressible Turbulent Channel Flow with Impedance Boundary Conditions," *Physics of Fluids*, Vol. 27, No. 3, 2015, Paper 035107. https://doi.org/10.1063/1.4914099

[9] Zhang, Q., and Bodony, D. J., "Numerical Investigation of a Honeycomb Liner Grazed by Laminar and Turbulent Boundary Layers," *Journal of Fluid Mechanics*, Vol. 792, April 2016, pp. 936–980. https://doi.org/10.1017/jfm.2016.79

[10] Avallone, F., Manjunath, P., Ragni, D., and Casalino, D., "Lattice-Boltzmann Very Large Eddy Simulation of a Multi-Orifice Acoustic Liner with Turbulent Grazing Flow," AIAA Paper 2019-2542, 2019. https://doi.org/10.2514/6.2019-2542

[11] Zhang, Q., and Bodony, D. J., "Numerical Simulation of Two-Dimensional Acoustic Liners with High-Speed Grazing Flow," *AIAA Journal*, Vol. 49, No. 2, 2011, pp. 365–382. https://doi.org/10.2514/1.J050597

[12] Shur, M., Strelets, M., Travin, A., Suzuki, T., and Spalart, P. R., "Unsteady Simulation of Sound Propagation in Turbulent Flow Inside a Lined Duct Using a Broadband Time-Domain Impedance Model," AIAA Paper 2020-2535, 2020. https://doi.org/10.2514/6.2020-2535

[13] Shur, M., Strelets, M., Travin, A., Suzuki, T., and Spalart, P., "Unsteady Simulations of Sound Propagation in Turbulent Flow Inside a Lined Duct," *AIAA Journal*, Vol. 59, No. 8, 2021, pp. 3054–3070. https://doi.org/10.2514/1.J060181

[14] Sebastian, R., Marx, D., and Fortuné, V., "Numerical Simulation of a Turbulent Channel Flow with an Acoustic Liner," *Journal of Sound and Vibration*, Vol. 456, Sept. 2019, pp. 306–330. https://doi.org/10.1016/j.jsv.2019.05.020

[15] Shahzad, H., Hickel, S., and Modesti, D., "Permeability and Turbulence over Perforated Plates," *Flow, Turbulence and Combustion*, Vol. 109, No. 4, 2022, pp. 1241–1254. https://doi.org/10.1007/s10494-022-00337-7

[16] Howerton, B. M., and Jones, M. G., "Acoustic Liner Drag: Measurements on Novel Facesheet Perforate Geometries," AIAA Paper 2016-2979, 2016. https://doi.org/10.2514/6.2016-2979

[17] Gaeta, R. J., and Ahuja, K., "Effect of Orifice Shape on Acoustic Impedance," AIAA Paper 2001-0662, 2001.
https://doi.org/10.2514/6.2001-662

[18] Bernardini, M., Modesti, D., Salvadore, F., and Pirozzoli, S., "STREAmS: A High-Fidelity Accelerated Solver for Direct Numerical Simulation of Compressible Turbulent Flows," *Computer Physics Communications*, Vol. 263, June 2021, Paper 107906.
https://doi.org/10.1016/j.cpc.2021.107906

[19] Bernardini, M., Modesti, D., Salvadore, F., Sathyanarayana, S., Della Posta, G., and Pirozzoli, S., "STREAmS-2.0: Supersonic Turbulent Accelerated Navier-Stokes Solver Version 2.0," *Computer Physics Communications*, Vol. 285, April 2023, Paper 108644.
https://doi.org/10.1016/j.cpc.2022.108644

[20] Chung, D., Chan, L., MacDonald, M., Hutchins, N., and Ooi, A., "A Fast Direct Numerical Simulation Method for Characterising Hydraulic Roughness," *Journal of Fluid Mechanics*, Vol. 773, June 2015, pp. 418–431.
https://doi.org/10.1017/jfm.2015.230

[21] MacDonald, M., Chung, D., Hutchins, N., Chan, L., Ooi, A., and Garca-Mayoral, R., "The Minimal-Span Channel for Rough-Wall Turbulent Flows," *Journal of Fluid Mechanics*, Vol. 816, April 2017, pp. 5–42.
https://doi.org/10.1017/jfm.2017.69

[22] Di Giorgio, S., Leonardi, S., Pirozzoli, S., and Orlandi, P., "On the Relationship Between Drag and Vertical Velocity Fluctuations in Flow over Riblets and Liquid Infused Surfaces," *International Journal of Heat and Fluid Flow*, Vol. 86, Dec. 2020, Paper 108663.
https://doi.org/10.1016/j.ijheatfluidflow.2020.108663

[23] Yang, J., Stroh, A., Chung, D., and Forooghi, P., "Direct Numerical Simulation-Based Characterization of Pseudo-Random Roughness in Minimal Channels," *Journal of Fluid Mechanics*, Vol. 941, June 2022, Paper A47.
https://doi.org/10.1017/jfm.2022.331

[24] Spalart, P. R., Moser, R. D., and Rogers, M. M., "Spectral Methods for the Navier-Stokes Equations with One Infinite and Two Periodic Directions," *Journal of Computational Physics*, Vol. 96, No. 2, 1991, pp. 297–324.
https://doi.org/10.1016/0021-9991(91)90238-G

[25] Vanna, F. D., Picano, F., and Benini, E., "A Sharp-Interface Immersed Boundary Method for Moving Objects in Compressible Viscous Flows," *Computers & Fluids*, Vol. 201, April 2020, Paper 104415.
https://doi.org/10.1016/j.compfluid.2019.104415

[26] Modesti, D., Sathyanarayana, S., Salvadore, F., and Bernardini, M., "Direct Numerical Simulation of Supersonic Turbulent Flows over Rough Surfaces," *Journal of Fluid Mechanics*, Vol. 942, July 2022, Paper A44.

[27] Modesti, D., Endrikat, S., Hutchins, N., and Chung, D., "Dispersive Stresses in Turbulent Flow over Riblets," *Journal of Fluid Mechanics*, Vol. 917, June 2021, Paper A55.
https://doi.org/10.1017/jfm.2021.310

[28] Endrikat, S., Modesti, D., Garca-Mayoral, R., Hutchins, N., and Chung, D., "Influence of Riblet Shapes on the Occurrence of Kelvin–Helmholtz Rollers," *Journal of Fluid Mechanics*, Vol. 913, April 2021, Paper A37.
https://doi.org/10.1017/jfm.2021.2

[29] Rayleigh, J. B., "On the Theory of Resonance," *Philosophical Transactions of the Royal Society of London*, Vol. 161, Dec. 1871, pp. 77–118.
https://doi.org/10.1098/rstl.1871.0006

[30] Ingård, U., "On the Theory and Design of Acoustic Resonators," *Journal of the Acoustical Society of America*, Vol. 25, No. 6, 1953, pp. 1037–1061.
https://doi.org/10.1121/1.1907235

[31] Guess, A., "Calculation of Perforated Plate Liner Parameters from Specified Acoustic Resistance and Reactance," *Journal of Sound and Vibration*, Vol. 40, No. 1, 1975, pp. 119–137.
https://doi.org/10.1016/S0022-460X(75)80234-3

[32] Tam, C. K. W., Ju, H., Jones, M. G., Watson, W. R., and Parrott, T. L., "A Computational and Experimental Study of Resonators in Three Dimensions," *Journal of Sound and Vibration*, Vol. 329, No. 24, 2010, pp. 5164–5193.
https://doi.org/10.1016/j.jsv.2010.06.005

[33] Zhang, Q., and Bodony, D. J., "Numerical Investigation and Modelling of Acoustically Excited Flow Through a Circular Orifice Backed by a Hexagonal Cavity," *Journal of Fluid Mechanics*, Vol. 693, Feb. 2012, pp. 367–401.
https://doi.org/10.1017/jfm.2011.537

[34] Schroeder, L., Spillere, A. M., Bonomo, L. A., da Silva, A. R., Avallone, F., and Cordioli, J. A., "Numerical Investigation of Acoustic Liners Experimental Techniques Using a Lattice-Boltzmann Solver," AIAA Paper 2021-2144, 2021.
https://doi.org/10.2514/6.2021-2144

C. Bailly
Associate Editor